Implementation of the Principle Phase Decomposition Algorithm

Erick Baziw, *Member, IEEE*

Abstract—This paper outlines the implementation details and enhancements of a previously described new concept in blind seismic deconvolution that is referred to as principle phase decomposition (PPD). A requirement of the PPD algorithm is for the investigator to determine the seismogram's dominant frequency (DF) and corresponding principle phase components (PPCs). Once these parameters are estimated, a hybrid Rao–Blackwellized particle filter and a hidden Markov model (HMM) filter are utilized to separate the potentially time-variant overlapping source wavelets. A variation of the PPD algorithm that is referred to as the PPD wavelet extraction (PPD-WE) technique addresses the requirement of estimating the seismogram's DF and PPCs. This paper describes in detail the PPD-WE algorithm where the overlapping source wavelets are sequentially and chronologically extracted from the seismogram under analysis. A HMM filter is described which facilitates in the simultaneous estimation of the DF and the corresponding phase of the source wavelet to be extracted within the PPD-WE algorithm. In addition, the utilization of the PPD-WE algorithm within standard frequency-domain deconvolution techniques is outlined.

Index Terms—Blind deconvolution, hidden Markov models (HMMs), jump processes, Rao–Blackwellized particle filter (RBPF).

I. INTRODUCTION

BLIND seismic deconvolution (BSD) is a very challenging and important seismic signal processing problem. The ability to blindly deconvolve an unknown source wavelet from an unknown reflection sequence has significant importance within many engineering disciplines such as civil, geotechnical, mining, and oil and gas exploration. The reflection coefficients identify and quantify the impedance mismatches between different geological layers. This information is of paramount importance when constructing civil structures and their associated foundations, monitoring the integrity of earth dams, exploring for minerals and oil and gas reserves, identifying primaries during passive seismic monitoring, and carrying out standard and passive seismic tomography investigations.

In seismology, the recorded time series $z(t)$ is defined to be the linear convolution of the source wavelet $S(t)$ with the Earth's reflection coefficients $\mu(t)$, with additive measurement noise $v(t)$. The mathematical representation of this relationship is given as

$$z(t) = \int\limits_0^t \mu(\tau) S(t-\tau) d\tau + v(t). \qquad (1)$$

The discrete representation of (1) is given as

$$z(k) = \sum_{i=1}^k \mu(i) S(k-i) + v(k), \qquad k = 1, 2, \ldots N. \quad (2)$$

As previously stated, BSD addresses the case where both $S(t)$ and $\mu(t)$ are unknown. A further complication in BSD relates to the case of a nonstationary source wavelet. It is readily known that the higher frequencies are attenuated more rapidly than lower frequencies resulting in significant variation in the source signal as it travels through the Earth.

Since BSD is a nonstationary and nonlinear optimal estimation problem, it requires algorithms that are structured to meet these requirements. Algorithms that are based upon Bayesian recursive estimation (BRE) techniques [where one estimates the posterior probability density function (pdf)] are ideally suited for solving nonlinear and time-varying physical problems. The state-of-the-art nonlinear BRE technique is the particle filter (PF) and its variants such as the Rao–Blackwellized particle filter (RBPF).

In [1], an innovative and powerful BRE-type algorithm for solving the BSD problem is outlined. This algorithm is referred to as principle phase decomposition (PPD). In the PPD formulation, all the associated filters of BRE (hidden Markov model (HMM) filter, Kalman filter (KF), PF, RBPF, and jump Markov systems) are implemented.

The PPD algorithm is shown to have many advantages such as simple filter formulation with minimal parameter specification, conducive to BSD, assumption of minimum phase source wavelet is not required, avoids problems associated with band-limited source wavelets as in the case of frequency-domain deconvolution, easily handles nonstationary source wavelets, provides for time-variant estimations of the source wavelet, relatively low associated computer computer-processing cost, reflection coefficients are not required to be represented by discrete state levels, and a whiteness assumption governing the reflection coefficient series is not required.

As outlined in [1], the main limitation in implementing the PPD algorithm is the requirement of specifying the dominant frequency (DF) and the corresponding principle phase

components (PPCs) of the seismogram. A variation of the PPD algorithm that is referred to the PPD wavelet extraction (PPD-WE) technique addresses this challenge. In the PPD-WE algorithm, the overlapping source wavelets are sequentially and chronologically extracted from the seismogram under analysis. This mitigates the requirement of prespecifying the DF and the corresponding PPC. The only DF and corresponding phase that are required to be specified are those of the current (in chronological order) source wavelet which is to be extracted from the seismogram. This information is readily available from the seismogram understudy.

Section III outlines the basic PPD-WE algorithm. In the test bed simulation results of Section III-A, a more advanced Monte Carlo technique is described which allows the investigator to vary the input filter parameters and subsequently obtain many estimates of the source wavelet under analysis. The source wavelet is then derived by averaging the results obtained from the Monte Carlo technique.

Section IV outlines the significant benefit of the PPD-WE technique in estimating the source wavelet for input into standard frequency-domain seismic deconvolution methodologies such as the water level technique (WLT) [2]. It is unlikely that the source wavelet will change significantly in stratigraphy such as pinch-out and thin bed layering. In this case, if the source wavelet is known, one can simply apply the WLT to obtain the desired reflection coefficients.

II. BACKGROUND

A. BRE

BRE is an optimal filtering technique that is based on state-space time-domain formulations of physical problems. Application of this type of filter requires that the dynamics of the system and measurement model, which relates the noisy measurements to the system state equations, be describable in a mathematical representation and probabilistic form which, with initial conditions, uniquely define the system behavior.

The potentially nonlinear discrete stochastic equation describing the system dynamics is defined as follows:

$$x_k = f_{k-1}(x_{k-1}, u_{k-1}) \leftrightarrow p(x_k|x_{k-1}). \quad (3)$$

In (3), the vector f_k is a function of the state vector x_k and the process or system noise u_k. It is assumed that (3) describes a Markov process of order one. The sampled potentially nonlinear measurement equation is given as

$$z_k = h_k(x_k, v_k) \leftrightarrow p(z_k|x_k). \quad (4)$$

In (4), h_k depends upon the index k, the state x_k, and the measurement noise v_k at each sampling time. The probabilistic state-space formulation described by (3) and the requirement for updating the state vector estimate based upon the newly available measurements described by (4) are ideally suited for the Bayesian approach to optimal estimation.

BRE is a two-step process consisting of prediction and update [3], [4]. In the prediction step, the system equation defined

by (3) is used to obtain the prior pdf of the state at time k via the Chapman–Kolmogorov equation, which is given as

$$p(x_k|z_{1:k-1}) = \int p(x_k|x_{k-1})p(x_{k-1}|z_{1:k-1})dx_{k-1}. \quad (5)$$

The Chapman–Kolmogorov is derived based upon the transitional densities of a Markov sequence. The update step computes the posterior pdf from the predicted prior pdf and a newly available measurement. The posterior pdf is updated via Bayes' rule as follows:

$$p(x_k|z_{1:k}) = \frac{p(z_k|x_k)p(x_k|z_{1:k-1})}{p(z_k|z_{1:k-1})}. \quad (6)$$

The recurrence equations that are defined by (5) and (6) form the basis for the optimal Bayesian solution. The BRE of the posterior density can be solved optimally (exact solution) when the state-space equations fit into a KF formulation or an HMM [3], [4]. Otherwise, BRE requires an asymptotically optimal numerical estimation approach such as sequential Monte Carlo filtering [3]–[6] when deriving the posterior pdf.

As previously stated, the standard set of KF equations can be implemented as an optimal solution to the BRE when certain conditions are met. These special conditions consist of the case where u_k and v_k are zero-mean independent Gaussian white noise processes, f_k is a linear function of the state vector and process noise, h_k is a linear function of the state vector and measurement noise, and the initial estimate of x_0 has a Gaussian distribution [3], [4].

Similar to the KF, a jump Markov linear Gaussian system (JMLGS) is also defined as a linear Gaussian system but in this case the system and/or measurement equations (f_k and h_k) evolve with time according to a finite-state Markov chain [7]–[9]. Table I outlines the KF governing equations for a JMLGS [1], [7], [10]. The index i that is denoted in Table I facilitates the implementation of a bank of KFs when implementing an RBPF (subsequently outlined). The HMM filter (also termed a grid-based filter) has a discrete state-space representation and has a finite number of states. In the HMM filter, the posterior pdf is represented by the delta function approximation [1], [3], [4], [10].

As stated previously, the recurrence equations that are defined by (5) and (6) form the basis for the optimal Bayesian solution and, except for the KF and HMM exact solutions, the BRE requires an asymptotically optimal numerical estimation approach. To solve the BRE numerically, a new family of filters that rely upon sequential Monte Carlo methods [3]–[6] have been made popular within the last decade. This family of new filters is most commonly referred to as PFs.

Similar to the HMM filter, the PF represents the posterior pdf by the delta function approximation, but in this case, a randomized grid is utilized for the estimation of the posterior pdf. For the PF, the particle weights are obtained using Bayesian importance sampling and a typical PF algorithm is generally referred to as sequential importance sampling (SIS) [3]–[6]. An important component of the PF algorithm is to carry out a particle degeneracy check. A common problem with the SIS approach is that after a few iterations, most particles have

TABLE I
KF GOVERNING EQUATIONS FOR JMLGS

Description	Mathematical Representation	Eq.
Finite state Markov chain.	$y_k^i \sim P\left(y_k^i \mid y_{k-1}^j\right)$	7
System equation.	$x_k^i = F(y_k^i)x_{k-1}^i + G(y_k^i)u_{k-1}^i$	8
Measurement equation.	$z_k^i = H(y_k^i)x_k^i + v_k^i$	9
State estimate extrapolation.	$\hat{x}_{k|k-1}^i = F(y_k^i)\hat{x}_{k-1|k-1}^i$	10
Error covariance extrapolation.	$P_{k|k-1}^i = F(y_k^i)P_{k-1|k-1}^i F(y_k^i)^T + G(y_k^i)Q_{k-1|k-1}^i G(y_k^i)^T$	11
Measurement extrapolation.	$\hat{z}_k^i = H(y_k^i)\hat{x}_{k|k-1}^i$	12
Innovation.	$\Delta_k^i = z_k^i - \hat{z}_k^i$	13
Variance of innovation.	$S_k^i = H(y_k^i)P_{k|k-1}^i H(y_k^i)^T + R_k^i$	14
Kalman gain matrix.	$K_k^i = P_{k|k-1}^i H(y_k^i)^T (S_k^i)^{-1}$	15
State estimate update.	$\hat{x}_{k|k}^i = \hat{x}_{k|k-1}^i + K_k^i \Delta_k^i$	16
Error covariance update.	$P_{k|k}^i = \left[I - K_k^i H(y_k^i)\right]P_{k|k-1}^i$	17

negligible weight (the weight is concentrated on a few particles only). This phenomenon is referred to as the degeneracy problem and it is due to the fact that the variance of the importance weights increases over time. A simple statistic to monitor which gives an indication of the degeneracy is the effective sample size N_{eff}. A small value of N_{eff} indicates severe degeneracy. The standard technique to counter the degeneracy problem is to resample the particles utilizing a Bayesian bootstrap technique [1], [3]–[6], [10] if the effective number of particles is less than a specified tolerance.

The RBPF allows for the reduction in the number of required particles when implementing BRE on nonlinear systems. The RBPF combines a bank of KFs with a PF. In this case, the KFs are utilized for generating a set of particles, where the weights of the particles are calculated with a PF [1], [7], [10]. In essence, the posterior pdf is approximated with a recursive stochastic mixture of Gaussians [1], [7], [10], [11]. This type of particle filtering algorithm is referred to as Rao–Blackwellization because it is related to the Rao–Blackwell theorem. The Rao–Blackwell theorem is named after Calyampudi Radhakrishna Rao and David Blackwell, and it describes a technique that transform a crude estimator into an estimator that is optimal by typically the mean-squared-error criterion [12].

In the RBPF implemented for the subsequently outlined algorithm, a set of particles are generated by, first, computing the finite-state Markov chain distribution (FSMCD), which is denoted as $P(y_k^i|y_{k-1}^i)$ in Table I. Second, based upon the samples drawn from $P(y_k^i|y_{k-1}^i)$, a bank of KFs (as outlined in Table I) is utilized to compute a set of particles. The posterior pdf of the state vector is then calculated and subsequent asymptotically optimal estimates are obtained.

B. PPD Algorithm Outline

In the PPD algorithm, the source wavelet is modeled as an amplitude modulated sinusoid (AMS) [1], [10], [13], [14]. The mathematical representation of an AMS is outlined as follows (continuous form):

$$x_1(t) = x_2(t)\sin[\omega t + \varphi] \tag{18}$$

where $x_1(t)$ is an approximation to the seismic source wavelet, $x_2(t)$ is the seismic wavelet's amplitude modulating term (AMT), ω is the DF of the wavelet, and φ is the corresponding phase.

As opposed to standard seismic deconvolution techniques that attempt to derive reflection coefficients, the PPD algorithm decomposes the seismogram into its associated overlapping source wavelets. This mitigates the problems connected to obtaining high bandwidth reflection coefficients from band-limited source wavelets [1]. The PPD algorithm also provides for time-varying estimations of the source wavelet.

The PPD algorithm implements a RBPF which individually weights and subsequently sums a bank of linear KFs with JMLGS. The KFs define the system and measurement dynamics for event and nonevent conditions [1]. The event condition is associated with the case of a source wavelet or overlapping source wavelets being present within the recorded time series at time index k. The nonevent condition represents the case when only measurement noise is present. As shown in Table I, the KFs are specified and updated (at each time increment) by samples drawn from an FSMCD. The FSMCD is defined by the probability and transitional probabilities of the event and nonevent conditions and it provides for a rich and diverse set of particles.

The major drawback of the PPD algorithm is that the investigator is required to initially specify the DF and the corresponding phases of the overlapping AMS source wavelets. This has proven to be a difficult task. To circumvent this limitation, a variant of the PPD algorithm is implemented where the overlapping source wavelets are sequentially and chronologically extracted from the seismogram under analysis. This new technique is referred to as the PPD-WE algorithm.

III. PPD-WE ALGORITHM OUTLINE

In the PPD-WE configuration, there are only two possible overlapping source wavelets, namely: 1) the source wavelet to be extracted (SWE) and 2) the remaining seismogram time series data. Furthermore, for each event condition, there are only two permutations. These permutations reflect the situation where only the source wavelet understudy is present at time index k [i.e., (1, 0)] and the case where the source wavelet understudy is overlapped with other time series data at time index k [i.e., (1, 1)]. The two-event condition allows the investigator to implement a significantly simplified PPD where only a three-state FSMCD (i.e., noise, event condition (1, 0) + noise, and event condition (1, 1) + noise) is required. This avoids the requirement of calculating the total number of overlapping source wavelet combinations [1]. The Appendix provides more

detail on the utilization of the three-state FSMCD within the PPD-WE.

In the PPD-WE filter formulation, the state equation defined in [1, eq. (21)] is slightly modified as follows:

$$
\begin{bmatrix} x1_{k+1} \\ x2_{k+1} \\ x3_{k+1} \\ x4_{k+1} \end{bmatrix} = \begin{bmatrix} 1 & \Delta & 0 & 0 \\ 0 & a_2 & 0 & 0 \\ 0 & 0 & 1 & \Delta \\ 0 & 0 & 0 & a_4 \end{bmatrix} \begin{bmatrix} x1_k \\ x2_k \\ x3_k \\ x4_k \end{bmatrix}
$$
$$
+ \begin{bmatrix} 0 & 0 & 0 & 0 \\ 0 & b_2 & 0 & 0 \\ 0 & 0 & 0 & 0 \\ 0 & 0 & 0 & b_4 \end{bmatrix} \begin{bmatrix} 0 \\ u2_k \\ 0 \\ u4_k \end{bmatrix}. \quad (19)
$$

The PPD-WE algorithm models the AMTs (states $x1_k$ and $x3_k$) of the AMS source wavelet with a first-order Taylor series approximation. The amplitude modulating terms defined in [1, eq. (21)] and (19) are forced to be positive by modifying the state estimate extrapolation equation (10) (see Table I) so that $\hat{\boldsymbol{x}}_{k|k-1}^i = |\boldsymbol{F}(y_k^i)\hat{\boldsymbol{x}}_{k-1|k-1}^i|$ for states $x1_k$ and $x3_k$. The AMT is set positive and the seismogram is also scaled (e.g., maximum amplitude of ±200 units) so that the sinusoidal term of the AMS accounts for source wavelet oscillations. The rate-of-change terms (states $x2_k$ and $x4_k$) are then approximated as Gauss–Markov processes. This allows for considerable flexibility and controllability when assigning prior to the amplitude modulating terms and for facilitating a greater diversity of particles (i.e., KFs).

The Gauss–Markov process has a relatively simple mathematical description. As in the case of all stationary Gaussian processes, specification of the process autocorrelation completely defines the process. The variance σ^2 and time constant T_c define the first-order Gauss–Markov process. The time constant terms (T_{c2} and T_{c4}, where $a_{2,4} = e^{-\Delta/T_{c2,4}}$) of states $x2_k$ and $x4_k$ are important parameters within the PPD-WE algorithm. It is desired that states $x2_k$ and $x4_k$ result in a smooth trajectory of the amplitude modulation terms of the AMS while at the same time allow for sufficient maneuverability so that the AMS source wavelet to be extracted (AMS-E) follows the oscillations of the user-specified sinusoid.

The PPD-WE applies a linear range of possible time constant terms equal to the number of specified particles (i.e., KFs) for states $x2_k$ and $x4_k$. In the subsequent test bed simulations, the range of time constant terms varies from 0.6 ms (i.e., $a_2 = a_4 = 0.92$, highly maneuverable) to 6.22 ms (i.e., $a_2 = a_4 = 0.992$, sluggish). The re-sampling portion of the PPD-WE indirectly estimates the optimal value of the time constant for states $x2_k$ and $x4_k$ within the range specified. This is accomplished by duplicating particles (KFs with associated T_cs) with significant weight and removing those with low weights.

The variances of states $x2_k$ and $x4_k$ (where $b_{2,4} = \sigma_{2,4}\sqrt{1 - e^{-2\Delta/T_{c2,4}}}$) are specified in a manner similar to the technique utilized in [14] and [15] when modeling nondeterministic forces such as the acceleration of a fighter plane in a dogfight with another plane. In this case, the acceleration standard deviation is chosen to be about 1/3 of the expected maximum acceleration. In specifying the variances of states $x2_k$ and $x4_k$, the PPD-WE algorithm identifies the approximate
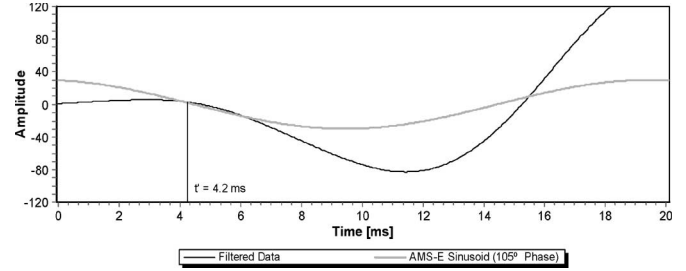

Fig. 1.   Illustration of a filtered synthetic seismogram with the AMS-E sinusoid and corresponding initial zero crossing of 4.2 ms shown.

maximum rate of change within the seismic time series under investigation and sets $\sigma_{2,4}^2$ to 1/9 of the square of this maximum.

The first-order Gauss–Markov measurement noise (i.e., state $x4_k$ in [1, eq. (21)]) has been removed from the system (19) due to the fact that the low-pass zero-phase-shift frequency filters applied to the seismogram greatly increases the signal-to-noise ratio. This mitigates the requirement of modeling Gauss–Markov measurement error. The measurement error of the PPD-WE algorithm is specified by parameter R_k defined in Table I.

The approach taken in simultaneously estimating the source wavelet's DF and corresponding phase is to implement an HMM filter similar to the HMM filters utilized to refine the AMS phases in the PPD technique [1]. In this PPD-WE filter formulation, a range of possible DFs (e.g., 30 to 70 Hz in 1-Hz increments) and corresponding phases is prespecified within a HMM filter formulation. As the data are processed, the HMM frequency estimation (HMM-FE) filter obtains an optimal estimate of the DF and the associated phase.

The PPD-WE measurement equation for the case when there is only the SWE present is given as

$$
z_k = x1_k \sin(\omega_k t + \varphi1_k) + v_k, \qquad \text{where } t = k\Delta. \quad (20)
$$

In (20), ω represents the DF of the SWE and $\varphi1_k$ is the corresponding phase at time index k (note: $H_k = [\sin(\omega_k t + \varphi1_k)\ 0\ 0\ 0]$). As outlined in [1], knowing the DF, one can easily obtain an initial estimate for the AMS-E sinusoid. For example, in Fig. 1, the DF of the AMS-E sinusoid is known to be 50 Hz and the initial phase is estimated to be 105° with a corresponding initial sinusoidal zero crossing of $t' = 4.2$ ms.

At the first zero crossing of the AMS-E sinusoid, we have the following relationship (for negative amplitude first break):

$$
\omega t' + \varphi1' = 180°. \quad (21)
$$

From (21), it is clear that there is a linear relationship between the DF and the corresponding phase at the first zero crossing denoted by t', which is given as

$$
\varphi1' = 180° - \omega t'. \quad (22)
$$

By utilizing (22), one can easily calculate a corresponding phase for any DF specified. For example, in the case outlined

in Fig. 1 ($t' = 4.2$ ms), a DF of 40 Hz would result in a corresponding phase of 119.5° and a DF of 70 Hz result in a corresponding phase of 74.2°.

Another important PPD-WE parameter to specify is the time index t_1 where it is assumed that the overlapping time series data have not yet arrived (i.e., only the AMS-E exist). This value is an approximation and is readily estimated as the end time of the AMS-E sinusoid initial phase estimate. For example, in Fig. 1, time index t_1 could be estimated to be approximately 7 ms. Alternatively, the investigator may already have prior knowledge of the minimal separation between reflection coefficients (Δt_r) and set $t_1 = t' + \Delta t_r$. Time index t_1 allows the PPD-WE to initially lock onto the AMS-E.

The following equation outlines the PPD-WE measurement equation for the BSD problem when it is assumed that a maximum of two source wavelets are overlapped at time index k for the event condition.

$$z_k = x1_k \sin(\omega_k k\Delta + \varphi1_k) + x3_k \sin(\omega_k k\Delta + \varphi3_k) + v_k. \tag{23}$$

In (23), parameters ω_k and $\varphi1_k$ denote the DF and the corresponding phase estimates of the source wavelet (obtained from the HMM-FE). The HMM filter phase estimate at time index k for time series data overlapping the SWE is defined by parameter $\varphi3_k$. The phase window resolution for $\varphi3_k$ is set at 1° to 360°.

Major advantages of the PPD-WE algorithm are the simplicity of implementation, minimal parameter specification, and there is no theoretical limit on the number of overlapping source wavelets. Table II outlines the PPD-WE filter formulation. A disadvantage of the PPD-WE algorithm is that any errors generated during the wavelet extraction process will propagate as the seismogram is sequentially and chronologically processed.

A. PPD-WE Simulation Results

There are slightly differing possible PPD-WE source wavelet estimation realizations depending upon the specification of the initial PPD-WE filter parameters of t', t_1, and R_k, and the utilization of Monte Carlo techniques to obtain realizations of $y_k^i \sim P(y_k^i | y_{k-1}^j)$ and jitter the particles (i.e., Step 4 of Table II). For this reason, a Monte Carlo technique is utilized which allows the investigator to vary the input filter parameters and subsequently obtain many estimates of the source wavelet. The source wavelet is then derived by averaging the subsequent PPD-WE source wavelet estimates.

In this PPD-WE technique (PPD-WEMC), an additional time parameter t_2 is introduced. Unfortunately, there are some situations where the AMT of the source wavelet will slowly start to diverge from the true value due to the degeneracy check. To mitigate this effect, the degeneracy check is turned off after time t_2 which results in a noisier estimated source wavelet but the diversity of the particles is maintained.

In the PPD-WEMC algorithm, the investigator initially specifies minimum $t'_{\min}$ (first seismogram zero crossing) and $t_{2\min}$ parameters. These parameters are modified within each

TABLE II
PPD-WE FILTER FORMULATION

Step	Description	Mathematical Representation
1	Scale seismogram (e.g., maximum amplitude of ±200 units). Identify the source wavelet to be extracted by specifying zero crossing t' and time index t_l (or alternatively Δt_r). Specify R_k (generally set at 1% of maximum amplitude of low-pass filtered seismogram). Specify the variance and time constant range for states $x2_k$ and $x4_k$. Based upon these parameter formulate the JMLGS system and measurement equations.	System Dynamics See (19). Measurement Equations See (20) for the case of 1 source wavelet. See (23) for the case of 2 overlapping source wavelets. Note: if no source wavelets present then $z_k = v_k$.
2	Specify N_S and initialize the prior and transitional pdf for the 3 state FSMCD as outlined in the Appendix.	$p(y_0^1), p(y_0^2), p(y_0^3),$ & $p(y_k^i | y_{k-1}^j)$ $i,j=1,2,3$
3	A. For HMM-FE specify the frequency window and resolution and initialize the prior and transitional pdfs for the fixed-grid DFs. B. For overlapping AMS phase interval $(\varphi3_k)$ initialize the prior and transitional pdfs for the fixed-grid phases	
4	At each time index, draw N_S samples for 3 state FSMCD. Update Kalman filter measurement equations based upon y_k^i as outlined in the Appendix .	$y_k^i \sim P(y_k^i | y_{k-1}^j)$ note: If $y_k^i = y_k^3$, then states $x1_k$ and $x3_k$ are jittered [16] (add on U[-1.5,+1.5]) to facilitate a diversity of particles.
5	Propagate sinusoids based upon current time index $t = k\Delta$ and phase estimates.	$sin(\omega_k t + \varphi l_k)$ & $sin(\omega_k t + \varphi3_k)$ where $t = k\Delta$
6	Utilizing (10)-(14) of Table 1 and updated sinusoids of Step 5, propagate the system and measurement equations, calculate importance weights[1] for particles and then update and normalize the weights.	$\widetilde{w}_k^i = w_{k-1}^i N(z_k | \hat{z}_k^i, S_k^i)$, $i = 1, ..., N_s$. $w_k^i = \widetilde{w}_k^i / \sum_{i=1}^{N_S} \widetilde{w}_k^i$
7	Obtain asymptotically optimal estimate of the state vector (AMS-E).	$\hat{x}_k \approx \sum_{i=1}^{N_S} w_k^i x_k^i$
8	Sampling Importance Re-sampling (SIR). Re-sample if $\hat{N}_{eff} < N_T$	$\hat{N}_{eff} = \dfrac{1}{\sum_{i=1}^{N_S} (w_k^i)^2}$
9	Use $\hat{x}_k$ and HMM filter equations to estimate ω_k and $\varphi3_k$.	
10	Utilize (15)-(17) of Table I to update the bank of KFs	
11	Let k = k+1 & iterate to step 4.	

1) de Freitas [7] demonstrates that the importance weights for y_k^i are given by the predictive density $p(z_k | z_{1:k-1}, y_{1:k}^i) = N(z_k ; \hat{z}_k^i, S_k^i)$, where N denotes a Gaussian distribution.
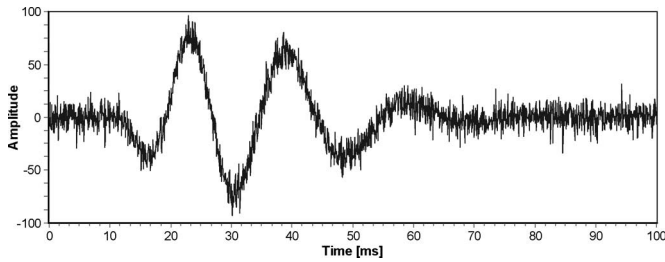
Fig. 2.   Synthetic seismogram generated by summing time-variant source wavelets BSW1, BSW2, BSW3, and BSW4.
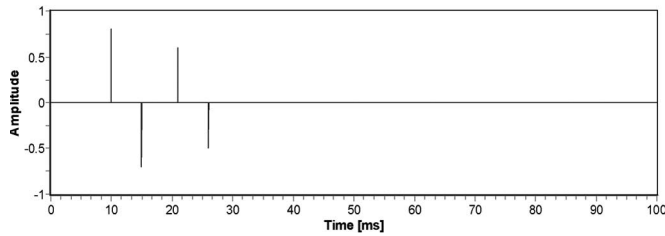

Fig. 3.   Reflection coefficients utilized to generate synthetic seismogram illustrated in Fig. 2.
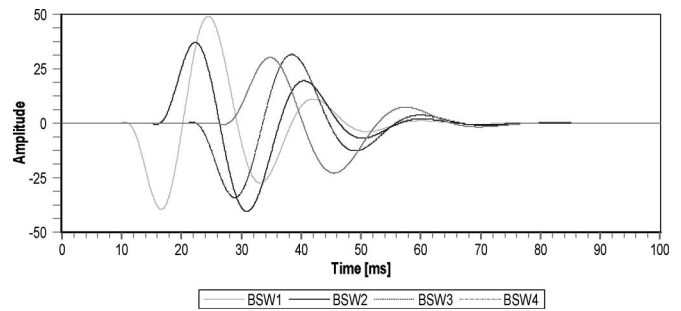

Fig. 4.   Output after convolving BSW1, BSW2, BSW3, and BSW4 with the first, second, third, and fourth reflection coefficients, respectively, shown in Fig. 3.
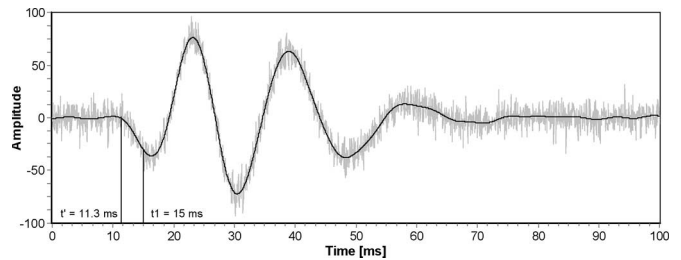

Fig. 5.   Output after applying a 200-Hz eighth-order zero-phase-shift low-pass Butterworth frequency filter to the synthetic seismogram shown in Fig. 2.
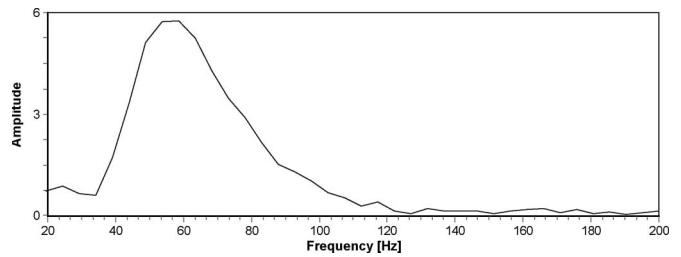

Fig. 6.   Amplitude spectrum of the seismogram illustrated in Fig. 2.

iteration of the PPD-MEMC algorithm (source wavelet estimate) according to the following two equations:

$$t' = t'_{\min} + \mathrm{abs}(t'') \tag{24}$$

$$t_2 = t_{2\min} + \mathrm{abs}(t'_2) \tag{25}$$

where $t'' \sim N(0, 0.4)$ and $t'_2 \sim N(0, 225)$. In addition, the measurement noise variance is increased from an initial user-specified minimum $R_{\min}$, according to a specified increment value R_{inc} (i.e., $R = R_{\min} + R_{\mathrm{inc}}$).

The implementation of the PPD-WEMC algorithm is outlined in more detail by considering a very challenging synthetic seismogram which contains time-variant source wavelets and two closely spaced dipoles. In this analysis, there are four overlapping source wavelets. The four overlapping source wavelets BSW1, BSW2, BSW3, and BSW4 are Berlage wavelets with DFs of $f = 55$ Hz, $f = 50$ Hz, $f = 45$ Hz, and $f = 40$ H, respectively, and parameters $n = 2$, $\alpha = 170$, and $\varphi = 60°$ [1] specified.

The synthetic seismogram illustrated in Fig. 2 was generated by convolving BSW1, BSW2, BSW3, and BSW4 with the first, second, third, and fourth reflection coefficients, respectively, shown in Fig. 3 and summing the results. The time series data illustrated in Fig. 2 have additive Gauss–Markov measurement noise with variance of 80 units^2 and a time constant of 0.01 ms. Fig. 4 illustrates BSW1, BSW2, BSW3, and BSW4 after implementing the previously described convolution process.

A 200-Hz eighth-order zero-phase-shift low-pass Butterworth frequency filter is then applied to the synthetic seismogram shown in Fig. 2 (to increase the seismogram's signal-to-noise ratio) to give the output illustrated in Fig. 5. Fig. 5 shows the filtered time series data superimposed upon the raw synthetic seismogram illustrated in Fig. 2. The time parameters $t'_{\min}$, t_1, and $t_{2\min}$ were estimated to be 11.3 ms, 15 ms (i.e., $\Delta t_r = 3.7$ ms), and 21 ms, respectively.

The amplitude spectrum of the seismogram shown in Fig. 2 is illustrated in Fig. 6. As is evident from Fig. 6, the dominant seismic bandwidth resides between 40 and 80 Hz. In the specification of the HMM-FE frequency range, it is mandatory that the investigator does not specify frequency values which incorporate the seismogram's overall frequency components. For example, the synthetic seismogram in Fig. 2 has overall frequency components ranging from 60 Hz (e.g., peak 1 to peak 3 and peak 2 to peak 4) to 70 Hz (e.g., peak 1 to peak 2). If these frequencies are incorporated into the HMM-FE, then the PPD-WE will just track the seismogram response and not the PPCs that comprise the seismogram.

In the implementation of the HMM-FE, an initial frequency range of 40–58 Hz was specified with an increment resolution of 0.1 Hz. This frequency range was based upon the spectrum illustrated in Fig. 6 and the requirement of avoiding frequency components between 60 and 70 Hz.

Additional parameters that are specified within the PPD-WEMC algorithm were $R_{\min} = 0.1$, $R_{\mathrm{inc}} = 0.15$, number of iterations $= 30$, and the number of particles (KFs) for each PPD-WE estimate was set to 500. The PPD-WE algorithm responds robustly to the number of particles specified. If there
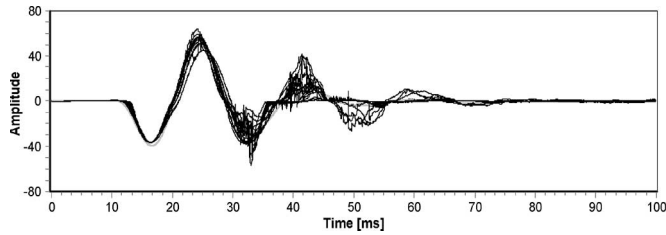
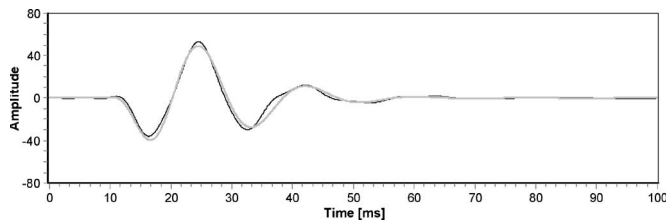Fig. 7.   PPD-WEMC estimated BSW1 source wavelets.

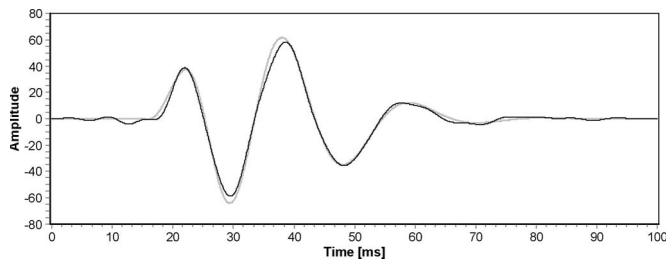Fig. 8.   Estimated and true BSW1 source wavelets.

Fig. 9. Estimated residual wavelet and the actual residual wavelet (i.e., BSW2 + BSW3 + BSW4).
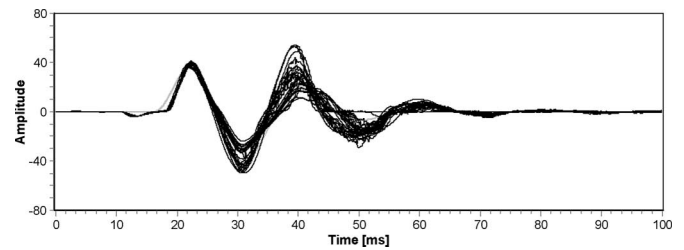

Fig. 10.   PPD-WEMC estimated BSW2 source wavelets.

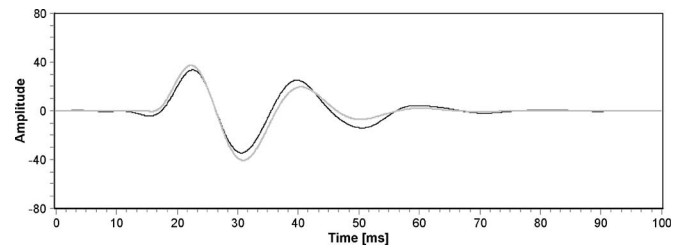Fig. 11.   Estimate and true BSW2 source wavelets.
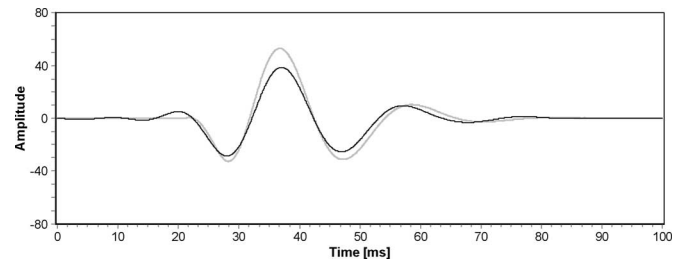
Fig. 12. Estimated residual wavelet and the actual residual wavelet (i.e., BSW3 + BSW4).

are CPU limitation concerns, the investigator can gradually lower the number of particles until consistent results are no longer obtained.

The PPD-WEMC algorithm provided for the AMS wavelet estimates illustrated in Fig. 7. Fig. 8 shows the estimated BSW1 source wavelet (black time series) and true BSW1 source wavelet (light gray time series). The estimated BSW1 source wavelet illustrated in Fig. 8 was generated by averaging the wavelets illustrated in Fig. 7 and applying a 150-Hz low-pass filter. As is evident from Fig. 8, the estimated and true BSW1 source wavelets are nearly identical.

Fig. 9 illustrates the estimated (black time series) residual wavelet and the actual (light gray time series) residual wavelet (i.e., BSW1 + BSW3 + BSW4). As is evident from Figs. 8 and 9, there is very close agreement between the estimated and true time series responses.

Subsequent to the extraction of the first arriving Berlage source wavelet (BSW1) illustrated in Fig. 8, the PPD-WEMC algorithm is then applied to the estimated residual wavelet shown in Fig. 9. In the second pass of the PPD-WEMC algorithm, the time parameters $t'_{\min}$, t_1, and $t_{2\min}$ were estimated to be 16.5, 21, and 28 ms, respectively.

The PPD-WEMC algorithm provided for the BSW2 AMS wavelet estimates illustrated in Fig. 10. Fig. 11 shows the estimated (black time series) and true (light gray time series) BSW2 source wavelets. The estimated BSW1 source wavelet illustrated in Fig. 11 was generated by averaging the wavelets

illustrated in Fig. 10 and applying a 150-Hz low-pass filter. As is evident from Fig. 11, the estimated and true BSW2 source wavelets are very close in agreement, but we start to see a gradual decrease in the quality in the estimate. This is due to the fact that any errors generated during the wavelet extraction process will propagate as the seismogram is sequentially and chronologically processed.

Fig. 12 shows the estimated (black time series) residual wavelet and the actual (light gray time series) residual wavelet (BSW3 + BSW4) where there is again a fairly close agreement between the estimated and true time series. There is also an indication of a decrease in the energy level of the estimated wavelet. The progressive performance limitation of the PPD-WEMC and PPD-WE algorithms is also due to the challenging nature of the problem (i.e., two closely spaced dipoles).

Subsequent to the extraction of Berlage source wavelets BSW1 and BSW2, the PPD-WE algorithm is then applied to the estimated residual wavelet shown in Fig. 12. In the third pass of the PPD-WEMC algorithm, the time parameters $t'_{\min}$, t_1, and $t_{2\min}$ were estimated to be 22.3, 28, and 35 ms, respectively. The HMM-FE frequency range was reduced to 40–50 Hz. This due to the fact that the estimated BSW2 wavelet had a peak frequency of 50 Hz and one would not expect a subsequently arriving source wavelet to have a greater frequency component.

The PPD-WEMC algorithm provided for the BSW3 AMS wavelet estimates illustrated in Fig. 13. Fig. 14 shows the
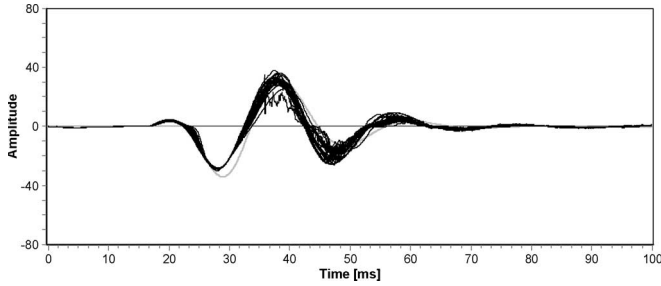
Fig. 13.   PPD-WEMC estimated BSW3 source wavelets.
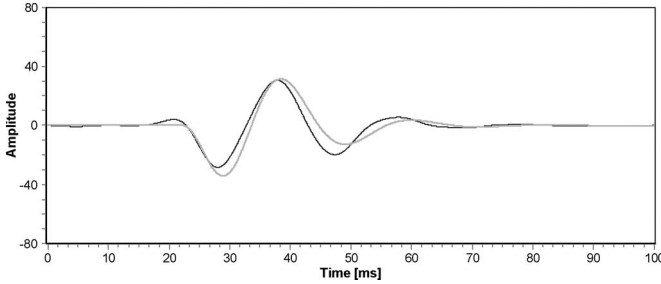

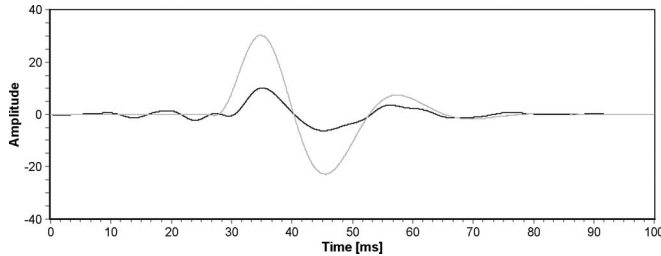Fig. 14.   Estimated and true BSW3 source wavelets.

Fig. 15.   Estimated and true BSW4 source wavelets.

estimated (black time series) and true (light gray time series) BSW3 source wavelets. The estimated BSW3 source wavelet illustrated in Fig. 14 was generated by averaging the wavelets illustrated in Fig. 13 and applying a 150-Hz low-pass filter. As is evident from Fig. 14, the estimated and true BSW3 source wavelets are close in agreement, but again there is evidence in the gradual decrease in the quality in the estimate.

Fig. 15 illustrates the estimated residual wavelet which is defined as Berlage source wavelet BSW4. As is evident from Fig. 15, there has been a significant decrease in the energy level of the estimated BSW4 source wavelet. Fig. 16 shows the normalized estimated (light gray time series) and true (black time series) source wavelets in Fig. 15. As is demonstrated in Fig. 16, the estimated BSW4 wavelet has a nearly identical form to the true wavelet. This information would be highly advantageous when carrying deconvolution on time series with a known source wavelet utilizing frequency-domain techniques. This is subsequently outlined in Section IV.

IV. UTILIZATION OF THE PPD-WE ALGORITHM WITHIN STANDARD FREQUENCY-DOMAIN DECONVOLUTION TECHNIQUES

A standard frequency-domain methodology in estimating the reflection series μ_k is the WLT [2]. If the measurement noise
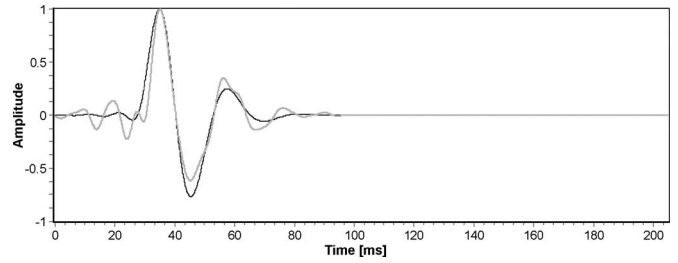

Fig. 16.   Estimated and true normalized BSW4 source wavelets.

term in (1) is ignored, then the Fourier transform of (1) is given as

$$z(t) = S(t) * \mu(t) \Leftrightarrow Z(\omega) = S(\omega)\Psi(\omega) \qquad (26)$$

rearranging terms gives

$$\Psi(\omega) = \frac{Z(\omega)}{S(\omega)}. \qquad (27)$$

Theoretically, for a known source wavelet, one could simply implement (27) and calculate $\Psi(\omega)$. The reflection series μ_k is then estimated by taking the inverse Fourier transform of $\Psi(\omega)$. Unfortunately, due to inaccuracies in the specification of the source wavelet, the band-limited nature of the source wavelet and additive measurement noise, the implementation of (27) is highly unstable and inaccurate.

To mitigate the previously outlined limitations, (27) is modified by, first, multiplying the numerator and denominator by the complex conjugate of $S(\omega)$ [denoted as $S^*(\omega)$] and, second, by introducing an additive scalar value to the denominator which is referred to as the *water level* (Δ) [2]. Implementation of these two modifications to (27) gives

$$\Psi(\omega) = \frac{Z(\omega)S^*(\omega)}{S(\omega)S^*(\omega) + \Delta} = \frac{Z(\omega)S^*(\omega)}{P_S(\omega) + \Delta} \qquad (28)$$

where $P_S(\omega)$ denotes the power spectrum of the source wavelet [i.e., the Fourier transform of the autocorrelation of $S(t)$]. In general terms, the setting of the water level is a trial-and-error approach. As $\Delta \rightarrow 0$, the resulting estimated reflection coefficients approach Dirac delta functions. When $\Delta \gg P(\omega)$, the resulting estimated reflection coefficients become significantly band limited and the result converges to the Fourier transform of the cross correlation between the recorded seismogram and the source wavelet [i.e., $Z(\omega)S^*(\omega)$].

The implementation of the WLT in conjunction with the PPD-WE technique is illustrated by considering the synthetic time series illustrated in Fig. 17. The simulated time series shown in this figure is a typical seismogram which one may encounter and it was generated without my prior knowledge of the source wavelet(s) or reflection series.

The amplitude spectrum of the seismogram shown in Fig. 17 is illustrated in Fig. 18. As is evident from Fig. 18, the dominant seismic bandwidth resides between 40 and 60 Hz.

A 200-Hz low-pass Butterworth frequency filter was then applied to the seismogram in Fig. 17 so that the signal-to-noise ratio was increased. The PPD-WE algorithm was then implemented on the filtered seismogram so that the first arriving
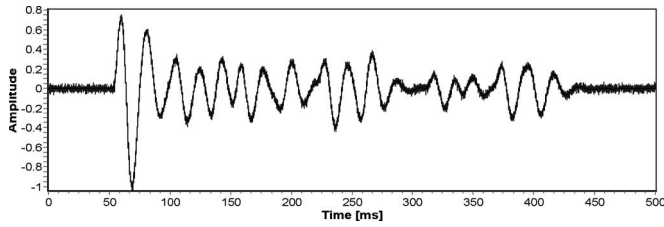
Fig. 17.   Typical synthetic seismogram.
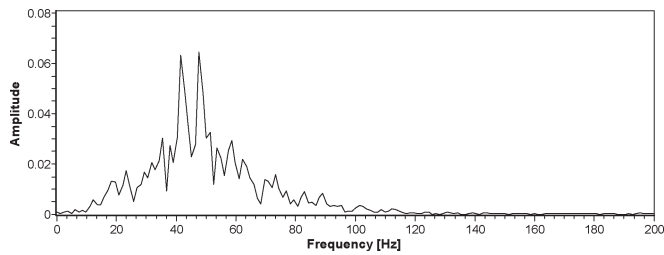

Fig. 18.   Amplitude spectrum of the seismogram illustrated in Fig. 17.
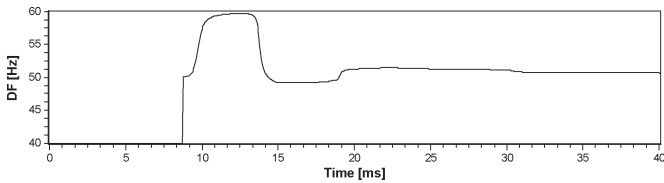

Fig. 19.   Illustration of the output of the HMM-FE filter after processing the filtered seismogram shown in Fig. 17.

source wavelet could be extracted and estimated. The first 45 ms of the filtered time series was ignored due to the fact no signal was present.

As a result of the estimated frequency bandwidth of the seismogram (i.e., Fig. 18), the HMM-FE component of the PPD-WE algorithm had a frequency range of 40–60 Hz specified. Fig. 19 illustrates the estimated DF output of the HMM-FE. As is evident from Fig. 19, the HMM-FE locks onto a DF range of approximately 49–51 Hz within 5 ms from the onset of the first arriving source wavelet.

Fig. 20 shows a single PPD-WE estimated first arriving source wavelet superimposed upon the true source wavelet. As is evident from Fig. 20, the PPD-WE algorithm estimated the correct DF of approximately 50 Hz and also did a very impressive job in estimating and extracting the first arriving source wavelet.

As opposed to going through the lengthy process of separating all possible overlapping source wavelets, the first deconvolution attempt was performed using the estimated source wavelet in Fig. 20 and the WLT. If there is minimal source wavelet variation within the time series, the estimated reflection coefficients will be very similar in shape. Fig. 21 illustrates the superimposition of the true reflection series onto the estimated reflection series for the synthetic seismogram shown in Fig. 17. For these results, an eighth-order Butterworth low-pass filter was applied to the noisy seismogram and the water level was set to 0.2% of the maximum value of the power spectrum of the seismogram. As is evident from Fig. 21, the WLT in conjunction with the PPD-WE algorithm did an excellent job in
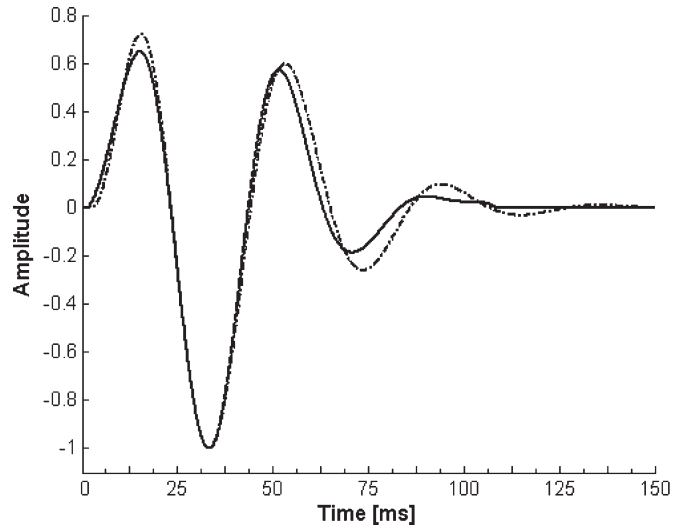

Fig. 20.   (Solid black line) estimated and (dotted line) true first arriving source wavelet.
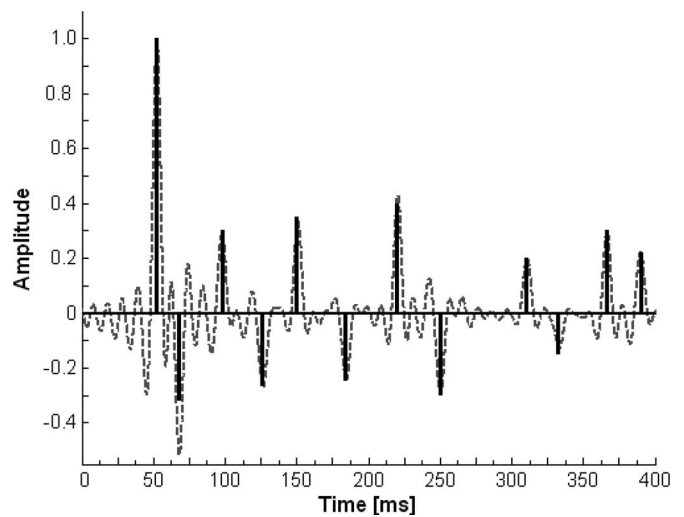

Fig. 21.   Superposition of (black line) the true reflection series onto (dotted line) the estimated reflection series.

recovering the true reflection series. In addition, we can assume that a stationary source wavelet is present due to the nearly identical shape of the estimated reflection coefficients.

The implementation of the PPD-WEMC algorithm on the seismogram illustrated in Fig. 17 provided for the source wavelet estimates illustrated in Fig. 22. Fig. 23 shows the estimated (black time series) and true (light gray time series) source wavelets. The estimated source wavelet illustrated in Fig. 23 was generated by averaging the wavelets illustrated in Fig. 22 and applying a 150-Hz low-pass filter.

As is evident from Fig. 23, the estimated and true source wavelets are nearly identical. The estimated responses after 62 ms would generally be ignored and are due to filter residual. Furthermore, it would physically not be expected for the source wavelet's energy level to significantly decay and subsequently buildup again. The filter residual corresponds to seismogram responses that have similar DF and phase components to that of the source wavelet under analysis.
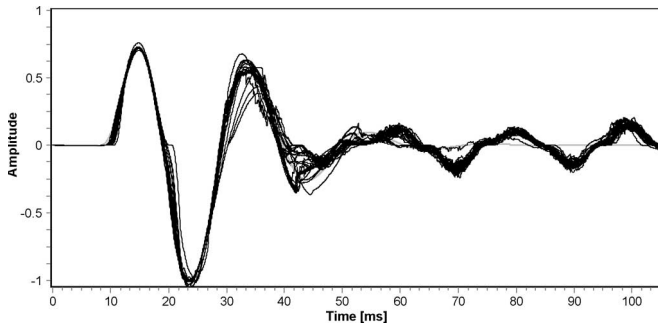
Fig. 22. PPD-WEMC estimated source wavelets for the seismogram shown in Fig. 17.
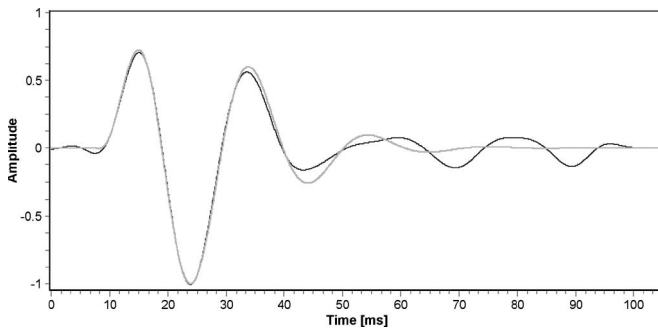

Fig. 23. Estimated and true source wavelets for the seismogram shown in Fig. 17.

V. CONCLUSION

This paper outlined the implementation details and enhancements of a previously described BSD technique that is referred to as PPD. An important component of the PPD technique is the modeling of the overlapping source wavelets as AMSs. The PPD algorithm utilizes RBPF, JMLGS, and HMM filters formulations to separate the overlapping wavelets according to their distinct DF and corresponding phase components.

The PPD algorithm has previously been shown to have many advantages such as simple filter formulation with minimal parameter specification, conducive to BSD, assumption of minimum phase source wavelet is not required, avoids problems associated with band-limited source wavelets as in the case of frequency-domain deconvolution, easily handles nonstationary source wavelets, provides for time-variant estimations of the source wavelet, relatively low associated computer computer-processing cost, reflection coefficients are not required to be represented by discrete state levels, and a whiteness assumption governing the reflection coefficient series is not required.

The main challenge in implementing the PPD algorithm is the specification of the DF and the corresponding PPCs of the seismogram. For this reason, a variation of the PPD algorithm that is referred to as the PPD-WE technique has been outlined in this paper. In the PPD-WE filter formulation, the overlapping source wavelets are sequentially and chronologically extracted from the seismogram under analysis. This mitigates the requirement of prespecifying the DFs and the corresponding PPCs. The only DF and corresponding phase which are required to be specified is that of the current (in chronological order)

source wavelet which is to be extracted from the seismogram. This information is readily available from the seismogram understudy.

The PPD-WE incorporates an HMM filter which simultaneously allows for both the estimation of the DF and the corresponding phase of the source wavelet. The ability to estimate the AMS DF makes the PPD-WE algorithm truly blind. An advanced Monte Carlo PPD-WE (PPD-WEMC) technique is also described in this paper which allows the investigator to vary the input filter parameters and subsequently obtain many estimates of the source wavelet under analysis. The source wavelet is then derived by averaging the results obtained from the PPD-WEMC algorithm.

The performance of the PPD-WE algorithm was demonstrated by considering a very challenging synthetic seismogram which contained time-variant source wavelets and two closely spaced dipoles. It was shown that the PPD-WE algorithm was able to separate the overlapping source wavelets. Major advantages of the PPD-WE algorithm are the simplicity of implementation, minimal parameter specification, and there is no theoretical limit on the number of overlapping source wavelets. A disadvantage of the PPD-WE algorithm is that any errors generated during the wavelet extraction process will propagate as the seismogram is sequentially and chronologically processed.

This paper also outlined the significant benefit of the PPD-WE technique in estimating the source wavelet for input into standard frequency-domain seismic deconvolution methodologies such as the WLT. It is unlikely that the source wavelet will change significantly in stratigraphy such as pinch-out and thin bed layering. In this case, if the source wavelet is known, one can simply apply the WLT to obtain the desired reflection coefficients.

APPENDIX
IMPLEMENTATION OF THE THREE-STATE FSMCD WITHIN THE PPD-WE ALGORITHM

The three states of the PPD-WE FSMCD $y_k^i \sim P(y_k^i | y_{k-1}^j)$ are measurement noise present at time index $k(p(y_k^1))$, the source wavelet understudy plus measurement noise present at time index $k(p(y_k^2))$, and the source wavelet understudy is overlapped with other time series data plus measurement noise at time index $k(p(y_k^3))$. As previously stated, a Markov chain is uniquely defined by the initial distribution and the transitional probabilities at time $k = 0$. For the simulations presented in this paper, the initial distribution for the three-state FSMCD was set to $p(y_0^1) = 0.5$, $p(y_0^2) = 0.4$, and $p(y_0^3) = 0.1$, respectively. This initial distribution is based upon the fact that at the start of the time series under analysis only measurement noise or the source wavelet understudy will be present (ability to window in on initial seismic wavelet recordings). The initial transitional probabilities were specified as

$$\begin{bmatrix} y_1^1|y_0^1 & y_1^1|y_0^2 & y_1^1|y_0^3 \\ y_1^2|y_0^1 & y_1^2|y_0^2 & y_1^2|y_0^3 \\ y_1^3|y_0^1 & y_1^3|y_0^2 & y_1^3|y_0^3 \end{bmatrix} = \begin{bmatrix} 0.1429 & 0.0357 & 0.0909 \\ 0.5714 & 0.3214 & 0.0909 \\ 0.2857 & 0.6429 & 0.8182 \end{bmatrix}. \quad (29)$$

These initial transitional probabilities were defined based upon the fact that the majority of the time series data under analysis would reflect the case where the source wavelet understudy is overlapped with other time series data plus measurement noise at time index k. It should also be noted that it is required that the columns of (29) add up to 1.0 according to the law of total probability.

At each time increment k, the pdf of the three-state FSMCD is updated according to the following equation:

$$
\begin{bmatrix} p\left(y_k^1\right) \\ p\left(y_k^2\right) \\ p\left(y_k^3\right) \end{bmatrix} = \begin{bmatrix} y_k^1|y_{k-1}^1 & y_k^1|y_{k-1}^2 & y_k^1|y_{k-1}^3 \\ y_k^2|y_{k-1}^1 & y_k^2|y_{k-1}^2 & y_k^2|y_{k-1}^3 \\ y_k^3|y_{k-1}^1 & y_k^3|y_{k-1}^2 & y_k^3|y_{k-1}^3 \end{bmatrix} \times \begin{bmatrix} p\left(y_{k-1}^1\right) \\ p\left(y_{k-1}^2\right) \\ p\left(y_{k-1}^3\right) \end{bmatrix}.
$$
(30)

The calculated probabilities $p(y_k^i)$ of (30) are sorted from lowest to highest. The Inverse Transform Method is then utilized to obtain realizations of the three-state FSMCD equal to the number of particles N_S specified by the investigator. In this step, a random number generator is utilized to obtain N_S samples of the uniform distribution $U^i[0,1]_k$ ($i = 1$ to N_S). The realizations of the three-state FSMCD are then calculated as follows:

$$
y_k^i = \begin{cases} y_k^1, & \text{if } U^i[0,1]_k < p\left(y_k^1\right) \\ y_k^2, & \text{if } p(y_k^1)U^i[0,1]_k < p\left(y_k^1\right) + p\left(y_k^2\right) \\ y_k^3, & \text{otherwise.} \end{cases}
$$
(31)

The realizations outlined in (31) are based upon the assumption that $p(y_k^1) < p(y_k^2) < p(y_k^3)$.

In terms of the JMLGS, the system (8) does not change but the measurement equation is updated based upon the estimated value of y_k^i. For the case $y_k^i = y_k^1$, the measurement equation is set equal to the background noise ($z_k = v_k$). For the case $y_k^i = y_k^2$, the measurement equation is defined by (20). For the case $y_k^i = y_k^3$, the measurement equation is set to (23) and states $x1_k$ and $x3_k$ are jittered [16] (i.e., add on $U[-1.5, +1.5]$) to facilitate a diversity of particles.

REFERENCES

[1] E. Baziw and T. J. Ulrych, "Principle phase decomposition—A new concept in blind seismic deconvolution," *IEEE Trans. Geosci. Remote Sens.*, vol. 44, no. 8, pp. 2271–2281, Aug. 2006.

[2] T. J. Ulrych and M. D. Sacchi, *Information-Based Inversion and Processing with Applications*. 1st ed. Amsterdam, The Netherlands: Elsevier, 2005.

[3] M. S. Arulampalam, S. Maskell, N. J. Gordon, and T. Clapp, "A tutorial on particle filters for online nonlinear/non-Gaussian Bayesian tracking," *IEEE Trans. Signal Process.*, vol. 50, no. 2, pp. 174–188, Feb. 2002.

[4] M. Mühlich, "Particle filters: A tutorial," in *Proc. Bucureşti Filter-Workshop*, Mar. 2003, pp. 1–45. [Online]. Available: www.uni-frankfurt.de/~muehlich/sci/TalkBucurestiMar2003.pdf

[5] A. Doucet, S. Godsill, and C. Andrieu, "On sequential Monte Carlo sampling methods for Bayesian filtering," *Stat. Comput.*, vol. 10, no. 3, pp. 197–208, 2000.

[6] A. Doucet, N. de Freitas, and N. Gordon, Eds., *Sequential Monte Carlo Methods in Practice*. New York: Springer-Verlag, 2001.

[7] N. de Freitas, "Rao–Blackwellised particle filtering for fault diagnosis," in *Proc. IEEE Aerosp. Conf.*, 2002, vol. 4, pp. 1767–1772.

[8] A. Doucet, N. J. Gordon, and V. Krishnamurthy, "Particle filters for state estimation of jump Markov linear systems," *IEEE Trans. Signal Process.*, vol. 49, no. 3, pp. 613–624, Mar. 2001.

[9] A. Doucet and C. Andrieu, "Iterative algorithms for state estimation of jump Markov linear systems," *IEEE Trans. Signal Process.*, vol. 49, no. 6, pp. 1216–1227, Jun. 2001.

[10] E. Baziw, "Real-time seismic signal enhancement utilizing a hybrid Rao–Blackwellized particle filter and hidden Markov model filter," *IEEE Geosci. Remote Sens. Lett.*, vol. 2, no. 4, pp. 418–422, Oct. 2005.

[11] A. Akashi and H. Kumamoto, "Random sampling approach to state estimation in switching environments," *Automatica*, vol. 13, no. 4, pp. 429–434, 1977.

[12] G. Casella and C. P. Robert, "Rao–Blackwellisation of sampling schemes," *Biometrika*, vol. 83, no. 1, pp. 81–94, 1996.

[13] E. Baziw and I. Weir-Jones, "Application of Kalman filtering techniques for microseismic event detection," *Pure Appl. Geophys.*, vol. 159, no. 1–3, pp. 449–473, Jan. 2002.

[14] E. Baziw, B. Nedilko, and I. Weir-Jones, "Microseismic event detection Kalman filter: Derivation of the noise covariance matrix and automated first break determination for accurate source location estimation," *Pure Appl. Geophys.*, vol. 161, no. 2, pp. 303–329, Feb. 2004.

[15] W. M. Lear, *Kalman Filtering Techniques*. Houston, TX: Lyndon B. Johnson Space Center, 1985, pp. 172–176. No. JSC-20688.

[16] F. Gustafsson, F. Gunnarsson, N. Bergman, U. Forssell, J. Jansson, R. Karlsson, and P. Nordlund, "Particle filters for positioning, navigation, and tracking," *IEEE Trans. Signal Process.*, vol. 50, no. 2, pp. 425–437, Feb. 2002.

Erick Baziw (M'05) received the B.A.Sc. degree in geophysics engineering and the M.A.Sc. degree in civil engineering from the University of British Columbia, Vancouver, BC, Canada, in 1986 and 1988, respectively, and the Ph.D. degree in geophysics time series analysis from the University of British Columbia, in 2007.

He is a Registered Professional Engineer in the disciplines of geophysics and software engineering. His research interests include Bayesian recursive estimation, signal processing, and imaging with a particular emphasis on blind seismic deconvolution, passive seismology, site characterization, seismic tomography, and instrument modeling.